Radiation pressure limits on the star formation efficiency and surface density of compact stellar systems

Roland M. Crocker [1]* Mark R. Krumholz,[1,2] Todd A. Thompson,[3] Holger Baumgardt [4] and Dougal Mackey[1,2]

[1]*Research School of Astronomy and Astrophysics, Australian National University, Canberra, ACT 2611, Australia*

[2]*Centre of Excellence for Astronomy in Three Dimensions (ASTRO-3D) 2611, Australia*

[3]*Department of Astronomy and Center for Cosmology & Astro-Particle Physics, The Ohio State University, Columbus, OH 43210, USA*

[4]*School of Mathematics and Physics, University of Queensland, Brisbane, QLD 4072, Australia*

ABSTRACT

The large columns of dusty gas enshrouding and fuelling star formation in young, massive stellar clusters may render such systems optically thick to radiation well into the infrared. This raises the prospect that both 'direct' radiation pressure produced by absorption of photons leaving stellar surfaces and 'indirect' radiation pressure from photons absorbed and then re-emitted by dust grains may be important sources of feedback in such systems. Here, we evaluate this possibility by deriving the conditions under which a spheroidal, self-gravitating, mixed gas-star cloud can avoid catastrophic disruption by the combined effects of direct and indirect radiation pressure. We show that radiation pressure sets a maximum star cluster formation efficiency of $\varepsilon_{\mathrm{max}} \sim 0.9$ at a (very large) gas surface density of $\sim 10^5 \, \mathrm{M_\odot \, pc^{-2}} \, (\mathrm{Z_\odot/Z}) \simeq 20 \, \mathrm{g \, cm^{-2}} \, (\mathrm{Z_\odot/Z})$, but that gas clouds above this limit undergo significant radiation-driven expansion during star formation, leading to a maximum stellar surface density very near this value for all star clusters. Data on the central surface mass density of compact stellar systems, while sparse and partly confused by dynamical effects, are broadly consistent with the existence of a metallicity-dependent upper limit comparable to this value. Our results imply that this limit may preclude the formation of the progenitors of intermediate-mass black holes for systems with $Z \gtrsim 0.2 \, \mathrm{Z_\odot}$.

Key words: hydrodynamics – instabilities – radiative transfer – ISM: jets and outflows – galaxies: ISM.

1 INTRODUCTION

It has been appreciated for some time that the direct radiation flux from young stars may be sufficiently intense to drive gas out of isolated protoclusters experiencing intense star formation. As such, direct radiation pressure – i.e. the momentum flux imparted by starlight to gas mediated via the photons' initial absorption and scattering by the dust borne by the gas – is an important agent of 'feedback' in such systems, a view supported by both observational (Scoville et al. 2001; Lopez et al. 2011, 2014) and theoretical (Krumholz & Matzner 2009; Fall, Krumholz & Matzner 2010; Murray, Quataert & Thompson 2010; Murray, Ménard & Thompson 2011; Skinner & Ostriker 2015; Thompson & Krumholz 2016) perspectives.

In this paper – which leaves off from developments in our previous paper on star-forming discs (Crocker et al. 2018, hereafter

CKTC18) which, in turn, follows Krumholz & Thompson (2012, 2013) – we show that *indirect* radiation pressure (i.e. radiation pressure due to dust-reprocessed photons rather than direct starlight photons; cf. Murray et al. 2010) will also, in many cases, have an important dynamical effect in nascent star clusters. Indirect radiation pressure effects arise because the molecular gas, from which stars form, bears dust that reradiates absorbed UV and optical light at infrared (IR) wavelengths. This same dust may – if it presents a sufficiently large column – subsequently scatter or absorb and reradiate the starlight down-scattered into the IR. Indeed, at the large gas and, consequently, dust columns concomitant to the intense star formation surface densities encountered in local ultraluminous IR galaxies (such as Arp 220) or in sub-mm galaxies at higher redshifts, a star-forming environment may be optically thick to photons with wavelengths as long $\sim$100 μm.[1] Most pertinent here, similar or even

---

[1]Fits to such galaxies' spectral energy distributions imply gas columns of $\sim$0.01–1 g cm^{-2} (Chakrabarti & McKee 2008), corresponding to optical depths of $\sim$10–100 at 20 μm and $\sim$1–10 at 100 μm.

* E-mail: Roland.Crocker@anu.edu.au

larger dust columns and consequent optical depths are also encountered in the densest star-forming clouds found in the Milky Way and other galaxies in the local Universe. For example, Clarkson et al. (2012) find that the stellar surface density in the central 0.4 pc of the Arches cluster near the Galactic Centre is ≈ 4 g cm^{-2}, and this is only a lower limit on the initial gas surface density, corresponding to optical depths of several at 100 µm. The young or still-forming superstar clusters in M82 (McCrady & Graham 2007) and NGC 253 (Leroy et al. 2018) have gas columns exceeding 10 g cm^{-2}, so at 100 µm the optical depth is ~ 10.

The existence of large optical depths at IR wavelengths in such systems raises the interesting possibility that, as the downshifted photons bang around inside the gas column, much more momentum can be extracted from them than is possible in the single-scattering limit pertinent to direct radiation pressure. Indeed, in the 'strong-trapping' limit the momentum per unit time extracted from starlight is amplified from L/c to $\sim \tau L/c$, where τ is the optical depth.[2] While such a trapped radiation field could in principle eject gas from galaxies (Murray et al. 2011), whether it does so in practice is a separate question. Both analytic calculations and simulations suggest that dust-reprocessed radiation pressure is a threshold effect: for a given column of gas and stars, there exists a critical maximum radiation flux that can be forced through the column while the gas remains in a stable hydrostatic equilibrium. As long as such an equilibrium exists, the gas plus radiation pressure forces self-adjust to be in balance with the gravitational force, and IR radiation pressure has little effect on the dynamics. Once the flux exceeds the critical value, however, the gas column becomes unstable and turbulent, and simulations show that the instability saturates into a state where the mass-averaged radiation force exceeds (though, as a result of radiation Rayleigh–Taylor instability, only slightly) the mass-averaged gravitational force, rendering the entire gas column super-Eddington and thus liable to ejection on a dynamical timescale (e.g. Davis et al. 2014; Tsang & Milosavljević 2015; Zhang & Davis 2017). Thus, the question of whether indirect radiation pressure is important for star formation reduces to the question of whether star-forming systems have combinations of gas column and radiative flux that place them into the stable and sub-Eddington regime or the unstable and super-Eddington one.

In CKTC18, we showed that the radiative flux in most star-forming discs, averaged over the entire star-forming disc, fall into the former rather than the latter category. Consequently, for the vast majority even of starbursting galaxies, radiation pressure cannot be an important regulator of star formation or driver of winds at galactic scales. On the other hand, as first shown by Thompson, Quataert & Murray (2005) and later confirmed in CKTC18, there is a very suggestive coincidence (cf. Andrews & Thompson 2011) between the upper boundary of the occupied region of the Kennicutt–Schmidt (KS) parameter space (of star formation surface density $\dot{\Sigma}_*$ vs gas surface density $\Sigma_{\rm gas}$) and the critical value of the star formation surface density ($\dot{\Sigma}_{*,\rm crit} \sim 10^3$ M$_\odot$ pc^{-2} Myr^{-1}, corresponding to a critical radiative flux of $F_{*,\rm crit} \sim 10^{13}$ L$_\odot$ kpc^{-2}) where indirect radiation pressure effects preclude hydrostatic equilibrium. This strongly suggests that, while indirect radiation pressure is not an important agent of feedback *on global scales* for most systems, it nevertheless circumscribes the parameter space along the locus of the KS relation that may be occupied by real systems. Moreover,

even if a star-forming system is globally sub-Eddington, the fact that star formation is highly clumpy can render individual star-forming subregions (i.e. nascent star clusters and superstar clusters forming out of individual giant molecular clouds) super-Eddington, driving outflows away from these subregions (Murray et al. 2011). Numerical exploration of this question in the context of the most massive star clusters, where the effect is expected to be most important, has been highly limited by computational costs. Skinner & Ostriker (2015) and Tsang & Milosavljević (2018) both simulate indirect radiation pressure effects in a forming star cluster, and find them to be quite modest, but they survey a very small part of parameter space, and one where, as we show below, indirect radiation pressure effects are not expected to be significant. Moreover, these authors adopt a constant opacity to indirect radiation pressure, an assumption that we showed in CKTC18 leads to fundamental changes in the dynamics of the problem. Motivated by the need to explore this problem over a wider range of parameters than simulations currently permit, here we direct our attention to the importance of indirect radiation and to its effects on local scales within regions experiencing intense star formation, e.g. individual molecular clumps that are collapsing to form stellar protoclusters or, in principle, larger stellar spheroids. Furthermore, we simultaneously incorporate *direct* radiation pressure effects in our model following the treatment of Fall et al. (2010, hereafter FKM10).

One might suspect that a threshold feedback mechanism such as indirect radiation pressure might be important for star-forming subregions because Hopkins et al. (2010) have compiled observations that support the existence of a universal, maximum *central*[3] surface mass density $\Sigma_{\rm max} \sim 10^5$ M$_\odot$/pc$^{-2} \simeq 20$ g cm^{-2} for spheroidal stellar systems across a span of ~ 7 orders of magnitude in total stellar mass M_* and ~ 5 in effective radius $R_{\rm e}$. These dense stellar systems include globular clusters in the Milky Way and nearby galaxies, massive star clusters in nearby starbursts, nuclear star clusters in dwarf spheroidals and late-type discs, ultracompact dwarfs, and galaxy spheroids spanning the range from low-mass 'cusp' bulges and ellipticals to massive 'core' ellipticals; these systems are all baryon-dominated and likely formed in rapid, dissipational events. Hopkins et al. (2010) have already weighed a number of theoretical scenarios that might explain the existence of a universal $\Sigma_{\rm max}$ including that it is an effect of IR radiation pressure mediated by dust. While seen as particularly promising by Hopkins et al. (2010), these authors did note that an explanation invoking indirect radiation pressure faces a number of challenges and further, recent work involving some of the original authors (Grudić et al. 2018a,b) seems to cast further doubt on this general scenario. The most significant challenge facing the scenario is presented by the differing metallicities of these systems and, therefore, the well-motivated expectation that their dust-to-gas ratio – and therefore IR opacity – should vary. In particular, one would expect *ceteris paribus* that systems that form their stars at quite high redshift and which are observed to have low stellar metallicities today, would have higher maximum surface densities. Other challenges include that the mechanism would seem not to work if the stellar content of the system were built up in a number of star formation events and that, again for systems formed at high redshift, there has been a lot of time for dynamical relaxation to diminish the central surface mass density. We revisit the question of whether the observed maximum

---

[2]Ultimately only bound, in principle, by energy conservation to $\lesssim (c/v) L$ where v is a characteristic velocity of the outflowing gas (e.g. Lamers & Cassinelli 1999).

[3]That is *not* the effective or mean surface density $M_*/(\pi R_{\rm e}^2)$ but the limiting surface mass density as $r \to 0$.

stellar surface density can in fact be explained by radiation pressure effects in this work.

In brief, this paper extends previous work in three ways: (i) we determine the stability curve for star forming, dusty clouds subject to radiation pressure deriving from the nascent stars adopting a realistic temperature-dependent opacity $\kappa \propto T^2$ (rather than assuming a constant value); (ii) we account simultaneously for direct and indirect radiation pressure effects; and (iii) we follow the evolution of star clusters (forming out of giant molecular clouds) accounting for radiation pressure in our determination of the final state surface mass density as a function of initial state surface mass density. The remainder of this paper is as follows. In Section 2, we present a theoretical calculation for the process of star formation limited by both direct and dust-reprocessed radiation. In Section 3, we compare this theoretical calculation to observations of star clusters, and discuss further implications of our findings. We summarize and conclude in Section 4.

1.1 A word on notation and symbols

To forestall any potential confusion, below we label (dimensionful and dimensionless) reference values of some general quantity x with a subscript asterisk: x_*. Thus, for instance, T_* is a reference (dimensionful) temperature and τ_* is a (dimensionless) reference optical depth (both defined below). Quantities connected to stars or star formation are labelled with a subscript '$\star$'. Thus, for instance, $M_\star$ is the total stellar mass of the system and $\dot{\Sigma}_{\star,\mathrm{crit}}$ is the critical star formation surface density (defined below).

2 RADIATION PRESSURE EFFECTS IN STAR-FORMING CLOUDS

Our goal in this section is to derive a theoretical model for the joint effects of direct and indirect radiation pressure feedback on a star-forming cloud. We begin in Section 2.1 by considering the effects of indirect radiation pressure, summarizing the relevant results from CKTC18 and adapting them from planar to spherical geometry. We then derive evolutionary tracks for star-forming clouds subject to indirect radiation pressure effects in Section 2.2. We extend this analysis to include the effects of direct radiation pressure, based on the treatment of FKM10, in Section 2.3.

2.1 Indirect radiation pressure

2.1.1 Recapitulation of CKTC18

The fundamental calculation in CKTC18 is as follows: for a specified planar column of self-gravitating, dusty gas, and stars with a specified turbulent velocity dispersion and internal radiation source, we search for a density and temperature profile that allows the system to be in simultaneous hydrostatic and radiative equilibrium. We then show that such equilibria exist if the radiation flux is below a critical value, and that radiation fluxes above this value destabilize the gas, causing it to become turbulent and driving much of it off in a wind. The system we consider in CKTC18 is, in the approximation that the local radiation spectrum is always well described by a Planck function and that dust and gas are dynamically well coupled, fully characterized by its surface densities of gas Σ_{gas} and stars $\Sigma_\star$, by the radiation flux per unit area provided by the stars[4]

---

[4]Of course, very similar considerations around, e.g. the stability (or not) of the gas column (see below), apply in the case that the radiative flux is

$F_\star$, and by the temperature-dependent Rosseland mean opacity of the dusty gas $\kappa_R(T)$; for $T \lesssim 150$–200 K, the opacity is well approximated by a power law $\kappa_R \propto T^2$ (Semenov et al. 2003).[5] From these dimensional quantities, CKTC18 (partially following Krumholz & Thompson 2012, 2013) show that one can define three dimensionless parameters that, together with the functional form of $\kappa_R(T)$, determine the stability of the system:

$$f_{\mathrm{gas}} = \frac{\Sigma_{\mathrm{gas}}}{\Sigma_{\mathrm{gas}} + \Sigma_\star} \tag{1}$$

$$\tau_* = \frac{1}{2}\Sigma_{\mathrm{gas}}\kappa_{R,*} \tag{2}$$

$$f_{\mathrm{E},*} = \frac{\kappa_{R,*}F_\star}{g_* c}, \tag{3}$$

where $T_* = (F_\star/ca)^{1/4}$ is the reference temperature at the top of the column, $\kappa_{R,*} = \kappa_R(T_*)$ is the opacity evaluated at this temperature, and $g_* = 2\pi G(\Sigma_{\mathrm{gas}} + \Sigma_\star)$ is the gravitational acceleration at the top of the column. Intuitively, the quantities f_{gas}, τ_*, and $f_{\mathrm{E},*}$ are the gas fraction, the effective optical depth, and the effective Eddington ratio, with the latter two quantities computed using the conditions that prevail at the top of the atmosphere. We emphasize that $f_{\mathrm{E},*}$ is distinct from $\langle f_{\mathrm{E}}\rangle$, which we define as the mass-weighted mean Eddington ratio throughout the gas column; the former is computed using conditions at the top of the gas column, while the latter is a mass-weighted mean over the gas column, and thus depends on the configuration of mass and radiation flux.

While $f_{\mathrm{E},*}$ and $\langle f_{\mathrm{E}}\rangle$ are physically distinct, CKTC18 show that the former determines the latter. For any specified gas fraction and optical depth, and for an opacity law $\kappa_R \propto T^2$ as expected at the temperatures relevant for star-forming molecular gas, there exists a maximum value of the Eddington ratio $f_{\mathrm{E},*} = f_{\mathrm{E,crit}}(\tau_*, f_{\mathrm{gas}})$, and thus a maximum radiation flux $F_\star$, at which such a gas column can be in hydrostatic balance.[6] If the system satisfies $f_{\mathrm{E},*} < f_{\mathrm{E,crit}}$, then the mass arranges itself into a vertical density profile for which $f_{\mathrm{E},*} < \langle f_{\mathrm{E}}\rangle < 1$, and the system is both stable and sub-Eddington. (We use the self-consistently calculated density – and consequent temperature – profiles from CKTC18 in the modelling presented in this paper.) If $f_{\mathrm{E},*} > f_{\mathrm{E,crit}}$, on the other hand, no equilibrium

---

dominantly supplied by an active galactic nucleus rather than star formation, but the physical context under consideration here is that of an isolated gas cloud collapsing to form a stellar cluster or super cluster; we therefore limit ourselves to consideration of the case that the radiative flux is supplied by stars.

[5]We show in Section A that the systems we consider in this paper satisfy this constraint.

[6]To be precise, CKTC18's calculation of $f_{\mathrm{E,crit}}(\tau_*, f_{\mathrm{gas}})$ depends on the assumption one makes about the efficiency of convective transport in regions where the column is unstable to convection, but where conventional convection is unable to carry a significant heat flux because radiation rather than gas dominates the enthalpy budget. CKTC18 derive values of $f_{\mathrm{E,crit}}(\tau_*, f_{\mathrm{gas}})$ for the two limiting cases of efficient convection (i.e. convection is able to carry enough heat to fully flatten the entropy gradient) and zero convective heat flux. (These two cases are labelled $f_{\mathrm{E,crit,c}}$ and $f_{\mathrm{E,crit,rt}}$, where c (rt) means convection (radiative transfer) governs the temperature profile.) The two differ substantially only at gas fractions above ≈ 50 per cent. For our purposes in this paper, we will mostly use the efficient convection limit, since simulations suggest reality lies closer to that case, only referencing the inefficient convection limit on occasion to point out the overall similarity of the results it produces. See CKTC18 for further discussion and cf. Section B.

matter profile is possible and, in fact, the system is unstable to the development of radiation Rayleigh–Taylor instability. Numerical simulations then show that in the saturated state of the instability $\langle f_E \rangle$ asymptotes to a value close to but just above unity, so that mass is slowly driven upward out of the gravity well by the radiation force. In physical units, for Milky Way dust opacity, and in a planar geometry, the condition that $f_{E,*} > f_{E,\,crit}$ and thus that gas be ejected is approximately equivalent to the condition that the radiation flux $F_\star \gtrsim 10^{13}\,\mathrm{L}_\odot\,\mathrm{kpc}^{-2}$ (a scale previously identified in Thompson et al. 2005) corresponding to a maximal star formation surface density $\sim 10^3\,\mathrm{M}_\odot\,\mathrm{pc}^{-2}\,\mathrm{Myr}^{-1}$.

2.1.2 *From planar to spherical geometry: limiting cases*

A gas cloud that is collapsing to form a star cluster will differ from the case considered in CKTC18 in that its geometry is primarily 3D rather than 2D. We must therefore extend the CKTC18 calculation from approximately planar to approximately spherical geometry. The column density of the cloud remains a critical variable, even in spherical geometry, because this is what will determine the run of temperature through the cloud, as first shown by Chakrabarti & McKee (2005, 2008), and the temperature determines the opacity and thus the radiation pressure force. A second issue to consider in spherical geometry is that the column density will not be uniform due to the clumpiness of the gas. However, we show in Appendix C that this has relatively modest effects, and induces uncertainties in our final results only at the factor of few level. However, the change from planar to spherical geometry none the less has an important effect on the stability of the system against indirect radiation pressure. While in spherical geometry the gravitational force and radiation *flux* both decline as $1/r^2$ (for r large enough that most of the mass is enclosed), the *force* exerted by indirect radiation pressure on gas at the surface of a cloud falls faster than $1/r^2$ because, as the cloud's radius expands, the dust temperature and opacity decline (again assuming that $T \lesssim 150$–200 K, so that we have $\kappa_R \propto T^2$). In terms of our dimensionless parameters, the key distinguishing characteristic of spherical geometry is that $\kappa_{R,*}$ is a decreasing function of cloud radius, so that $f_{E,*}$ falls with radius as well. This differs from the planar case, for which there is no flux divergence and thus the opacity goes to a fixed, non-zero value as $z \to \infty$, rather than dropping to zero, so that $f_{E,*}$ is constant. It also differs from the case of the direct radiation force treated in FKM10 and that we shall revisit below, where the opacity is determined by the colour temperature of the stellar sources and thus is independent of distance.

Because the indirect radiation force in spherical geometry drops with radius faster than the gravitational force, there is no maximum flux beyond which it becomes impossible for a gas column to remain hydrostatic. At sufficient distance, the IR radiation force always drops to zero (in terms of our dimensionless parameters, $f_{E,*} \to 0$), and thus for a sufficiently extended spherical configuration a solution that looks like a pressure-supported atmosphere always exists. (Recall that this statement applies only to the IR force; we will address the question of the direct radiation force below.) In light of this discussion, we can ask what happens to a star-forming cloud that, as a result of a rising luminosity as gas transforms into stars, begins to violate the planar stability condition derived by CKTC18 at its surface (i.e. $f_{E,*} > f_{E,\,crit}$ using the radiation flux and surface density evaluated at the cloud radius r). If $f_{E,*} > f_{E,\,crit}$ in planar geometry, then the mass-weighted mean Eddington ratio $\langle f_E \rangle > 1$, and there is no way that the system can return to a sub-Eddington

state as long as the flux remains fixed. For spherical geometry, on the other hand, a system that has $\langle f_E \rangle > 1$ at its starting radius will at some point expand enough to have $\langle f_E \rangle < 1$, because $f_{E,*}$ will drop below $f_{E,\,crit}$. We can imagine two limiting outcomes for what will happen in this case.

Type A (disruption): any time a spherical cloud finds itself in a configuration with $f_{E,*} > f_{E,\,crit}$, it expands violently, leaving it vulnerable to rapid disruption by something else: hydrodynamic stripping by background flows, loss of mass from supernovae, stellar winds, or direct radiation pressure, or by tidal stripping. Under this assumption, a cloud that becomes super-Eddington is assumed to disrupt almost immediately.

Type B (quasi-equilibrium expansion): a cloud that finds itself with $f_{E,*} > f_{E,\,crit}$ undergoes quasi-equilibrium expansion as needed in order to remain marginally stable, $f_{E,*} = f_{E,\,crit}(\tau_*, f_{gas})$, at its instantaneous gas fraction and luminosity. It will continue to form stars until it is disrupted by direct radiation pressure or some other mechanism.

While neither of these two limiting cases for cloud evolution is likely to exactly describe the messy, non-linear reality of cloud expansion under radiation pressure, they will bracket reality. Moreover, as we show below, expressed in terms of an efficiency defined as the ratio of final to initial surface density, they lead to rather similar results. We spend a few sentences here, however, discussing which scenario is likely to be closer to the truth. This basically comes down to a question of relative timescales. The timescale for the surface density to change is a dynamical time. However, the timescale for the temperature and thus opacity to change is significantly smaller than that, because the timescale to reach thermal equilibrium is the radiation diffusion time, which is the size of the system divided by the characteristic diffusion speed of c/τ. Thus, the thermal equilibrium time is $\tau r/c$, which is smaller than the crossing time by a factor of $c/(\tau v) \gg 1$. Thus to good approximation, the opacity that the radiation field sees adjusts instantaneously (with respect to the dynamical time).

The remaining question is whether, in a cloud that finds itself at a luminosity such that it exceeds the stability limit at its current radius, gas is accelerated rapidly enough to exceed the escape speed before it has time to move far enough out in radius for the spherical divergence of the radiation field to reduce the force back below the Eddington limit. For indirect radiation pressure mediated by IR radiation and powered by star formation, the answer to this is likely 'no' and for the following reason: suppose we have a cloud with initial radius r and surface gravitational acceleration g, which finds itself slightly super-Eddington because ongoing star formation makes the radiation flux passing through it large enough that $f_{E,*} > f_{E,\,crit}$. It will only remain super-Eddington until the material is able to expand significantly, so the condition for disruption is, roughly, that the gas be accelerated to above the escape speed before the radius changes by a factor of order unity. Suppose further that the net outward acceleration of the material is a_{net}, which we can write in terms of an effective Eddington ratio for the accelerating gas as $a_{net} \simeq (\langle f_E \rangle - 1)g$. Thus by the time the gas propagates from r to $2r$, its velocity will be $v \simeq \sqrt{2r(\langle f_E \rangle - 1)g}$. The escape speed from radius r is $\sqrt{2gr}$, and from $2r$ it is $\sqrt{gr}$. Thus, the condition that $v > v_{esc}$ is satisfied only if $\sqrt{2(\langle f_E \rangle - 1)} > 1$. However, numerical simulations of super-Eddington dusty atmospheres show that, as a result of RRT instability, $\langle f_E \rangle$ is very close to unity even when gas is unstable and being ejected (Krumholz & Thompson 2012, 2013; Davis et al. 2014; Tsang & Milosavljević 2015; Zhang & Davis 2017), so that $\langle f_E \rangle - 1 \ll 1$. This in turn means that the IR radiation will not be sufficient to raise gas to the escape speed over

a distance of radius r.[7] Thus, while we certainly expect some gas to be driven out of a system as it forms stars, the effect of indirect radiation pressure in dusty, star-forming (spherical) clouds can be largely characterized as causing a quasi-equilibrium expansion to lower surface mass density (i.e. the 'Type B' scenario). Of course, this picture is complicated if there are other sources of feedback acting but, as we show below, even accounting for direct radiation pressure effects, this general picture does not change too much.

2.2 Evolutionary tracks with indirect radiation pressure

With the preceding discussion in mind, we now adapt our previous work to the case of spherical, self-gravitating, and star-forming molecular clouds. With R the cloud radius, the total (cross-sectional) surface mass density is

$$\Sigma_{\rm tot} = \Sigma_\star + \Sigma_{\rm gas} = \frac{M_{\rm tot}}{\pi R^2} = \frac{M_\star}{(1 - f_{\rm gas})\,\pi R^2}, \quad (4)$$

where, in the last equality, we utilize the gas (mass) fraction $f_{\rm gas}$. The surface gravity is

$$g_* = \frac{G M_{\rm tot}}{R^2}. \quad (5)$$

The luminosity of a simple stellar population of mass $M_\star$ and age t that fully samples the initial mass function (IMF) can be approximated by $L_\star \simeq \Psi M_\star/\max(1, t/t_{\rm cr})$ (Krumholz & Dekel 2010; CKTC18), where Ψ is the light-to-mass ratio of a zero age stellar population, and $t_{\rm cr}$ is the time required for the population to reach statistical equilibrium between an increase in luminosity from new stars forming and a decrease from older stars going out. For a Chabrier IMF, $\Psi = \Psi_0 \approx 2200$ erg s^{-1} g^{-1} ≈ 1100 L$_\odot$ M$_\odot^{-1}$ and $t_{\rm cr} = t_{\rm cr,\,0} \approx 6.9$ Myr.[8] Since the radiation pressure effects we investigate here are expected to have set the final mass configuration within a nascent cluster at $t \ll t_{\rm cr}$, i.e. well before its radiative output reaches the statistical equilibrium regime,[9] we henceforth write

---

[7] Note that this argument applies only if changes in the radiative flux occur on timescales that are not fast compared to the timescale over which the gas can dynamically readjust so as to maintain $\langle f_{\rm E} \rangle \sim 1$. This condition is satisfied for systems where the power source is star formation, since the radiation flux provided by stars cannot increase much faster than the dynamical time of the system. However, it might not be satisfied for active galactic nuclei, where changes in the accretion behaviour of the small inner accretion disc can drive luminosity increases on timescales much shorter than the dynamical time of the vastly larger dusty torus. Also note the situation here is quite different to the direct radiation scenario explored in Thompson & Krumholz (2016). In that case, radiation pressure can drive out significant amounts of material because a non-negligible fraction of material (in low column regions) finds itself super-Eddington by a factor $\gtrsim 2$; such does not occur in the simulations of indirect radiation pressure. There might be some tail of fast-moving material that gets accelerated to escape speed, but the bulk certainly is not.

[8] Formally, $t_{\rm cr} \equiv \Phi/\Psi$, where $\Phi = 4.1 \times 10^{17}$ erg g^{-1} $\approx 6.7 \times 10^9$ L$_\odot$ (M$_\odot$ yr^{-1})$^{-1}$ is the light-to-mass ratio for a stellar population in statistical equilibrium between star formation and stellar death (Kennicutt & Evans 2012). To presage later discussion, if the typical IMF varies with environment or evolves with cosmic time or with location because, e.g. of metallicity effects, then so, too, will the typical Ψ. Moreover, even if the universe realizes an approximately constant IMF, because this is itself uncertain (e.g. Murray 2009), Ψ must itself be considered to be uncertain. Binarity effects – not accounted for in this estimate of Ψ_0 – might also be important.

[9] On the basis of the modelling by Skinner & Ostriker (2015), we expect a cluster to have formed and its gas dispersed before $\approx 10\tau_{\rm ff}$ where $\tau_{\rm ff}$ is the freefall time. Conservatively normalizing to a cluster of relatively

---

$L_\star \simeq \Psi M_\star$. The temperature of the cloud surface is

$$T_* = \left(\frac{F_\star}{ca} \right)^{1/4} = \left(\frac{\Psi M_\star}{4\pi R^2 ca} \right)^{1/4}. \quad (6)$$

With these equations, we can now write the optical depth and Eddington ratio as

$$\tau_* = \frac{\kappa_{R,*} M_{\rm gas}}{4\pi R^2} = \frac{f_{\rm gas}}{(1 - f_{\rm gas})} \frac{\kappa_0}{8 T_0^2} \left(\frac{\Psi \Sigma_\star^3}{ca} \right)^{1/2} \quad (7)$$

$$f_{\rm E,*} = \frac{\kappa_{R,*} F_\star}{gc} = \frac{(1 - f_{\rm gas})\,\kappa_0}{8\pi G T_0^2} \left(\frac{\Psi^3 \Sigma_\star}{c^3 a} \right)^{1/2}, \quad (8)$$

respectively, where we have normalized the opacity by defining

$$\kappa_R(T) = \kappa_0 \left(\frac{T}{T_0} \right)^2. \quad (9)$$

For solar metallicity, $\kappa_0 \approx 10^{-1.5}$ cm^2 g^{-1} for $T_0 = 10$ K. Note that $M_\star$ drops out of both τ_* and $f_{\rm E,*}$; also note that, although the centre-to-edge column density $M/4\pi R^2$ is the quantity that determined τ_*, we have chosen to parameterize our system in terms of the projected column density $\Sigma = M/\pi R^2$, because this is the observable quantity to which we are interested in comparing.

2.2.1 The stability limit

If we now set

$$f_{\rm E,*} = f_{\rm E,crit}(\tau_*, f_{\rm gas}), \quad (10)$$

with $f_{\rm E,*}$ evaluated from equation (8) and $f_{\rm E,\,crit}$ as calculated numerically in CKTC18 (using equation 7 for τ_*), then for any given stellar surface density $\Sigma_\star$ we can solve numerically for the gas fraction $f_{\rm gas,\,crit}$ at which the cloud transitions from stable to unstable against indirect radiation pressure effects. Clouds that have gas fractions $f_{\rm gas} > f_{\rm gas,\,crit}$ are unstable to indirect radiation pressure, while those with $f_{\rm gas} < f_{\rm gas,\,crit}$ are stable. Although it is possible to express all our results in terms of gas fraction, it is more intuitive to instead consider a cloud that began its evolution consisting entirely of gas, with surface density Σ_0, and whose stellar surface density $\Sigma_\star$ is a result of subsequent star formation. In this case, the gas fraction is simply related to the star formation efficiency ε by

$$\epsilon = 1 - f_{\rm gas} = \Sigma_\star/\Sigma_0. \quad (11)$$

Thus at fixed stellar surface density, clouds that have already processed a large fraction of their gas into stars ($\varepsilon \approx 1$) are more stable than those that have processed little gas into stars ($\varepsilon \ll 1$), with the two regimes separated at a critical efficiency $\varepsilon_{\rm crit} = 1 - f_{\rm gas,\,crit}$. We show these two regimes and the value of $\varepsilon_{\rm crit}$ that separates them in Fig. 1 (with the uncoloured region marked 'allowed' showing the stable zone of parameter space, and the blue shaded 'excluded' region showing the unstable zone); the numerical evaluation used in the plot is for solar metallicity.

In Fig. 1, we also show trajectories in the plane of $(\Sigma_\star, \varepsilon)$ taken by spherical, star-forming clouds evolving at constant total surface mass densities of $\Sigma_0 = 10^{4.5}$ M$_\odot$ pc^{-2}, $\Sigma_{0,crit} \equiv 1.3 \times 10^5$ M$_\odot$ pc^{-2}, and 5×10^5 M$_\odot$ pc^{-2}; we define $\Sigma_{0,\,crit}$ in detail below. Since $\Sigma_\star = \varepsilon \Sigma_0$, in a log–log plot these trajectories are simply

---

low volumetric mean density $\langle \rho_\star \rangle = 10^5$ M$_\odot$/(5 pc^3) $\simeq 190$ M$_\odot$ pc^{-3}, we have $\tau_{\rm ff} = [3\pi/(32G\rho)]^{1/2} \sim 6 \times 10^5$ yr, so even for this extremal (for our purposes) case we have a formation time $t < t_{\rm cr}$.
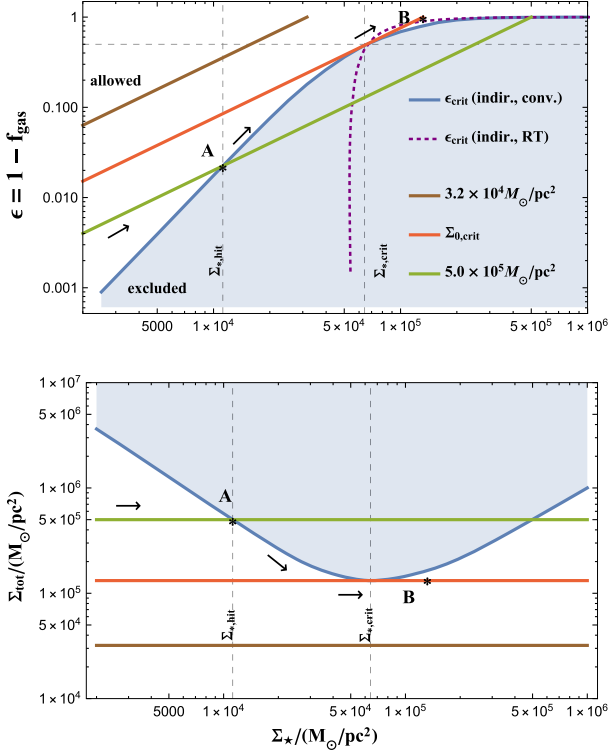
Figure 1. Star formation efficiency ε (top) and total surface density Σ_{tot} (bottom) as a function of stellar surface density $\Sigma_{\star}$ for gas of solar metallicity accounting solely for indirect radiation pressure effects. The blue curve is defined by the condition $f_{\text{E},\star} = f_{\text{E, crit}}$ (equation 10), with $f_{\text{E, crit}}$ set equal to the result of CKTC18's case of efficient convection; the shaded blue region, labelled 'excluded', is the part of parameter space where clouds are unstable to indirect radiation pressure. For comparison, the dashed purple curve shows the separation between stable and unstable assuming no convection. The solid green, red, and brown lines show trajectories taken by star-forming clouds with different, fixed total mass surface density (Σ_0) as indicated; the star formation efficiency and stellar surface densities for these clouds are related by $\varepsilon = \Sigma_{\star}/\Sigma_0$, and clouds evolve from lower left to upper right in the top panel as they form stars. Dashed vertical black lines indicate stellar surface densities $\Sigma_{\star,\text{hit}}$ (defined in Section 2.2.2) and $\Sigma_{\star,\text{crit}}$ (equation 14), and the dashed horizontal black line shows $\varepsilon = 1/2$; the significance of the points 'A' and 'B' is also described in Section 2.2.2.

lines of slope unity, with a vertical offset determined by Σ_0. Clouds begin their lives in the lower left corner of the plot, and as they convert gas into stars they move to the upper right. Comparing these cloud trajectories to the stability curve for indirect radiation pressure, it is clear that we can distinguish two types of trajectory. Clouds with small initial surface densities, such as the one whose evolutionary path is illustrated by the brown line in Fig. 1, can convert all of their gas into stars without encountering the stability line; indirect radiation pressure effects, therefore, do not limit the gas-to-stars conversion efficiency in such systems. However, direct radiation pressure effects *do* limit the eventual stellar surface density as described in Section 2.2.2. Clouds with larger values of the initial gas surface density Σ_0, as illustrated for example by the green line in Fig. 1, will eventually encounter the stability line once they have converted enough of their mass to stars. This cloud becomes unstable once it reaches the stellar surface density where the green curve intersects the blue stability line, at the point marked A in the plot; we calculate the stellar surface density at which

this occurs in the next section. These two regimes are separated by a critical initial surface density $\Sigma_0 = \Sigma_{0,\text{crit}} \simeq 1.3 \times 10^5\ M_\odot$ pc^{-2} (at solar metallicity),[10] which corresponds to $\Sigma_0 = \Sigma_{0,\text{crit}}$, i.e. the value of Σ_0 such that the cloud trajectory is tangent to the stability curve (shown by the red line in Fig. 1 that grazes the blue stability curve at $\Sigma_{\star} = \Sigma_{\star,\text{crit}}$ indicated by the right vertical dashed line). We can derive an accurate approximation to $\Sigma_{0,\text{crit}}$ analytically as follows. The first step is to obtain an analytic approximation to the stability curve shown by the blue line in Fig. 1. We do so making use of an analytical approximation derived in CKTC18:

$$f_{\text{E, crit}} \simeq \frac{1 - f_{\text{gas}}}{\tau_\star}. \tag{12}$$

With this approximation, and making use of equations (7) and (8), we can express the stability curve as

$$\Sigma_{\star,\text{crit}} \simeq \Sigma_{\star,\text{char}} \sqrt{\frac{\epsilon}{1 - \epsilon}}, \tag{13}$$

where

$$\Sigma_{\star,\text{char}} \equiv \frac{8\sqrt{\pi G a c}\, T_0^2}{\kappa_0 \Psi}$$

$$\simeq 13.4\ \text{g cm}^{-2} \left(\frac{\kappa_0}{10^{-1.5}\ \text{cm}^2\ \text{g}^{-1}}\right)^{-1} \left(\frac{\Psi}{\Psi_0}\right)^{-1}. \tag{14}$$

Armed with this expression, it is straightforward to find the critical value of Σ_0 at which the stability curve is tangent to a cloud trajectory $\Sigma_{\star,\text{cloud}} = \epsilon \Sigma_0$, since this just amounts to the requirements that $\Sigma_{\star,\text{crit}} = \varepsilon \Sigma_0$ and

$$\frac{d\Sigma_{\star,\text{crit}}}{d\epsilon} = \frac{d\Sigma_{\star,\text{cloud}}}{d\epsilon} = \Sigma_0. \tag{15}$$

With a bit of algebra, one can show that the solution is $\varepsilon = 1/2$, and plugging this into the approximation for the stability curve, equation (13), immediately gives

$$\Sigma_{\star,\text{crit}} \simeq \Sigma_{\star,\text{char}} \tag{16}$$

and

$$\Sigma_{0,\text{crit}} = \Sigma_{\star,\text{crit}}/\epsilon \simeq 2\Sigma_{\star,\text{char}} = \frac{16\sqrt{\pi G a}\, c T_0^2}{\kappa_0 \Psi}$$

$$\simeq 27.6\ \text{g cm}^{-2} \left(\frac{\kappa_0}{10^{-1.5}\ \text{cm}^2\ \text{g}^{-1}}\right)^{-1} \left(\frac{\Psi}{\Psi_0}\right)^{-1}$$

$$\simeq 1.3 \times 10^5\ M_\odot\ \text{pc}^{-2} \left(\frac{\kappa_0}{10^{-1.5}\ \text{cm}^2\ \text{g}^{-1}}\right)^{-1} \left(\frac{\Psi}{\Psi_0}\right)^{-1}. \tag{17}$$

Assuming – as is indicated by many observations (Leroy et al. 2011; Santini et al. 2014; Accurso et al. 2017) – that the dust-to-gas ratio scales directly with the gas metallicity at least down to metallicities of ≈ 10 per cent of solar, and also assuming that dust properties are similar to those determined locally, these generalize to

$$\Sigma_{0,\text{crit}}(Z) \simeq 1.3 \times 10^5\ M_\odot\ \text{pc}^{-2} \left(\frac{Z}{Z_\odot}\right)^{-1} \left(\frac{\Psi(Z)}{\Psi_0}\right)^{-1}, \tag{18}$$

where $\Psi = \Psi(Z)$ acknowledges the possibility that there could be metallicity-dependent evolution of the light-to-mass ratio because, e.g. of systematic IMF changes with Z.

---

[10]This is the value for $f_{\text{E, crit}} = f_{\text{E, crit, c}}$. In the case that $f_{\text{E, crit}} = f_{\text{E, crit, rt}}$, we find $\Sigma_{0,\text{crit,rt}} \simeq 1.2 \times 10^5\ M_\odot\ \text{pc}^{-2}$, nearly identical. (See footnote 6 for the meanings of $f_{\text{E, crit, c}}$ and $f_{\text{E, crit, rt}}$.)

2.2.2 Evolutionary tracks for unstable clouds

What happens if $\Sigma_0 > \Sigma_{0,\mathrm{crit}}$ as for the green curve in Fig. 1? In this case, the cloud trajectory will hit the stability curve (as does the example green curve, at the point A in Fig. 1) at some stellar surface density $\Sigma_{\star,\mathrm{hit}} < \Sigma_{\star,\mathrm{char}}$ (indicated by the left vertical line in Fig. 1). We can solve numerically for the intersection point $\Sigma_{\star,\mathrm{hit}}$, and the corresponding star formation efficiency $\varepsilon_{\mathrm{hit}}$ at this point in the cloud's evolution, by solving equation (10) simultaneously with $\Sigma_\star = \varepsilon \Sigma_0$ using our tabulated stability curve $f_{\mathrm{E,crit}}(\tau_\ast, f_{\mathrm{gas}})$. We can obtain an analytic approximation to this solution using the approximate stability curve given by equation (13), which yields

$$\Sigma_{\star,\mathrm{hit}} = \epsilon_{\mathrm{hit}} \Sigma_0 \simeq \Sigma_{\star,\mathrm{char}} \sqrt{\frac{\epsilon_{\mathrm{hit}}}{1 - \epsilon_{\mathrm{hit}}}}. \tag{19}$$

The solution is

$$\Sigma_{\star,\mathrm{hit}} \simeq \frac{\Sigma_{0,\mathrm{crit}}}{2} \sqrt{\frac{\chi - \sqrt{\chi^2 - 1}}{\chi + \sqrt{\chi^2 - 1}}} \tag{20}$$

$$\epsilon_{\mathrm{hit}} \simeq \frac{1}{2} \left(1 - \sqrt{1 - \chi^{-2}} \right), \tag{21}$$

where $\chi \equiv \Sigma_0 / \Sigma_{0,\mathrm{crit}} > 1$. The stellar surface density $\Sigma_{\star,\mathrm{hit}}$ is the x-coordinate of A in Fig. 1, and $\varepsilon_{\mathrm{hit}}$ is the y-coordinate of A in the upper panel of Fig. 1.

From this point, two evolutionary paths, type A and type B as identified above, are possible. In the case where a cloud expels its gas and ceases star formation as soon as it becomes unstable (type A), the final efficiency for conversion of gas into stars is simply $\varepsilon_{\mathrm{f}} = \varepsilon_{\mathrm{hit}}$, and the corresponding stellar surface density is $\Sigma_{\mathrm{f}} = \varepsilon_{\mathrm{f}} \Sigma_0$; the end point of such an evolutionary history is indicated by the asterisk labelled 'A' in Fig. 1. The second evolutionary path (type B) is one wherein the cloud expands in order to maintain marginal stability, and is illustrated by the arrows in Fig. 1. In this case, a cloud begins evolving at constant Σ_{tot}, and thus along a line of slope unity described by $\varepsilon = \Sigma_\star/\Sigma_0$. However, once the cloud hits the stability line at $\Sigma_{\star,\mathrm{hit}}$, it cannot continue to evolve at constant Σ_{tot}. Instead, it travels *along* the marginal stability curve, which corresponds to expanding in radius while the star formation efficiency increases. It remains on this curve, at the edge of stability, until reaching the tangent point at $\Sigma_\star \simeq \Sigma_{\star,\mathrm{char}}$, $\epsilon \simeq 1/2$, at which point it can continue its evolution at a new constant surface density $\Sigma_{\mathrm{tot}} = \Sigma_{0,\mathrm{crit}}$. If indirect radiation pressure were the only effect limiting star formation, the cloud would then proceed to form stars at this surface density until it converted all its mass to stars and reached a final star formation efficiency $\varepsilon_{\mathrm{f}} = 1$; the endpoint of such a trajectory is indicated by the 'B' in Fig. 1. In this case, the final stellar surface density is simply $\Sigma_{\mathrm{f}} = \Sigma_{0,\mathrm{crit}}$. We will see in the next section that the effects of direct radiation pressure alter this conclusion, though only slightly.[11]

2.3 Evolutionary tracks with direct radiation pressure

As presaged above, we next incorporate *direct* radiation pressure effects following FKM10. For direct radiation pressure, the critical luminosity at which gas is expelled corresponds to that which delivers enough momentum within one dynamical time to drive the atmosphere to roughly the escape speed. FKM10 show that the required luminosity is

$$L_{\mathrm{crit,dir}} = \alpha_{\mathrm{crit}} \frac{Gc(1-\epsilon)M_{\mathrm{tot}}^2}{5\eta f_{\mathrm{trap}} R^2}, \tag{22}$$

where $f_{\mathrm{trap}} \sim 2$–5 accounts for assistance from main-sequence winds and incomplete leakage of starlight and wind energy (Krumholz & Matzner 2009), α_{crit} is a parameter of order unity that accounts for magnetic support and turbulent support, and $\eta = 2/(4-k)$[12] where the internal density profile of the cloud follows $\rho \propto r^{-k}$; following FKM10, we adopt a fiducial $\eta = 2/3$ and consider $f_{\mathrm{trap}}/\alpha_{\mathrm{crit}}$ in the range $1/4$–4. We can rewrite this critical luminosity in terms of a flux at the surface cloud surface by dividing both sides by $4\pi R^2$:

$$F_{\mathrm{crit,dir}} = \alpha_{\mathrm{crit}} \frac{\pi}{20} \frac{Gc}{\eta f_{\mathrm{trap}}} f_{\mathrm{gas}} \Sigma_{\mathrm{tot}}^2$$

$$= \alpha_{\mathrm{crit}} \frac{\pi}{20} \frac{Gc}{\eta f_{\mathrm{trap}}} \frac{f_{\mathrm{gas}} \Sigma_\ast^2}{(1-f_{\mathrm{gas}})^2} . \tag{23}$$

Now equating the stellar radiation flux $F = \Psi M_\star/(4\pi R^2) = \Psi \Sigma_\star/4$ to the critical flux, we obtain a critical stellar surface density required for direct radiation pressure force to eject the gas and halt star formation:

$$\Sigma_{\ast,\mathrm{crit,dir}} = \frac{5}{\pi} \frac{\eta f_{\mathrm{trap}} \Psi}{\alpha_{\mathrm{crit}} Gc} \frac{(1-f_{\mathrm{gas}})^2}{f_{\mathrm{gas}}}$$

$$= \frac{5}{\pi} \frac{\eta f_{\mathrm{trap}} \Psi}{\alpha_{\mathrm{crit}} Gc} \frac{\epsilon^2}{1-\epsilon} . \tag{24}$$

Defining a characteristic scale for stellar surface density due to direct radiation pressure effects

$$\Sigma_{\star,\mathrm{char,dir}} \equiv \frac{5}{\pi} \frac{\eta f_{\mathrm{trap}} \Psi}{\alpha_{\mathrm{crit}} Gc}$$

$$\simeq 5900 \ \mathrm{M_\odot \ pc^{-2}} \left(\frac{\eta}{2/3} \right) \left(\frac{f_{\mathrm{trap}}}{\alpha_{\mathrm{crit}}} \right) \left(\frac{\Psi}{\Psi_0} \right), \tag{25}$$

we can solve equation (24) to find (taking the positive root)

$$\epsilon_{\mathrm{crit,dir}}(\Sigma_\star) = \frac{\Sigma_\star}{2\Sigma_{\star,\mathrm{char,dir}}} \left[\left(1 + \frac{4\Sigma_{\star,\mathrm{char,dir}}}{\Sigma_\star} \right)^{1/2} - 1 \right]; \tag{26}$$

(this equation is equivalent to FKM10, equation 6). Some example curves for $\varepsilon_{\mathrm{crit,dir}}(\Sigma_\star)$ are shown in yellow in Fig. 2, with the shaded yellow region indicating the part of parameter space where clouds are unstable to disruption by direct radiation pressure.

---

[11]Note here that we are defining final stellar surface density simply as the total mass in stars formed divided by the final cross-sectional area. In reality, for a type B evolutionary path stars that form before the cloud becomes unstable to indirect radiation pressure could form in a more compact configuration than stars that form later, after the cloud has begun expanding. In principle, we could use a more sophisticated definition of surface density that weights by mass formed in different phases of the evolution. However, such an estimate could differ from our simple one by at most a factor of ≈ 2, because half of the total mass in stars (or slightly less once direct ra-

diation pressure is included) forms after the cloud reaches a total surface density $\Sigma_{0,\mathrm{crit}}$. Given the simplicity or our model overall, the extra algebraic complexity required to capture this factor of 2 effect does not seem warranted.

[12]Note that $k > -4$ is required for the similarity solution presented by Krumholz & Matzner (2009); a different similarity solution for $k \leq -4$ can be obtained, but such a steep density profile does not seem physically relevant and we do not consider it further.
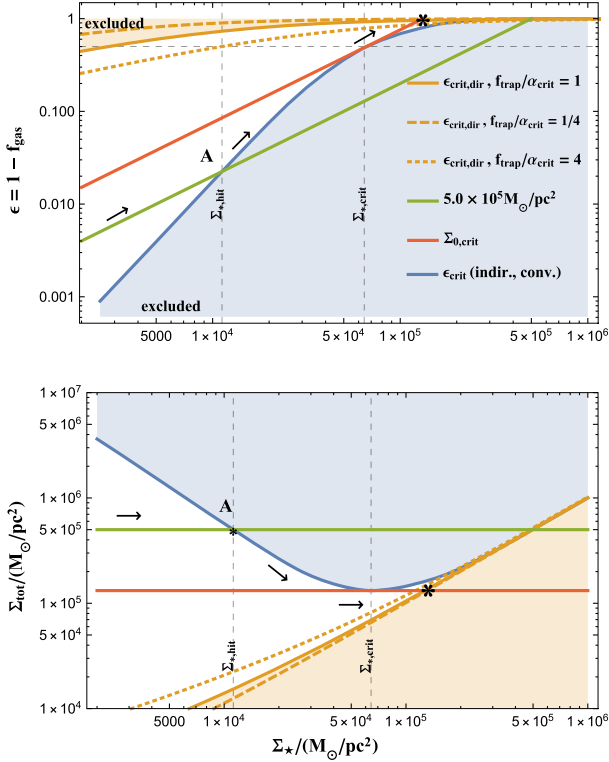
Figure 2. Star formation efficiency ε (top) and total surface density Σ_{tot} (bottom) as a function of stellar surface density $\Sigma_\star$, incorporating both direct and indirect radiation pressure effects. The plots adopt $\Psi = \Psi_0$. The blue shaded region shows the locus within which clouds are unstable against indirect radiation pressure (for solar metallicity), while the yellow shaded region shows the locus of instability against direct radiation pressure (for $\eta = 2/3$ and the indicated values of $f_{trap}/\alpha_{crit} = 1$). The green line shows an example trajectory at fixed $\Sigma_0 = 5 \times 10^5 \, M_\odot \, pc^{-2} > \Sigma_{0,\,crit}$, while the red line shows an example trajectory with $\Sigma_0 = \Sigma_{0,crit}$. Arrows show the path taken by a cloud that expands while forming stars so as to remain marginally stable against indirect radiation pressure.

Note that, unlike for indirect radiation pressure, once the $(\Sigma_\star, \varepsilon)$ configuration of the system crosses the $\varepsilon_{crit,\,dir}(\Sigma_\star)$ critical line, direct radiation pressure invariably blows out the remaining gas in the system, cutting off further star formation. The cloud cannot stabilize by expanding as it can for indirect radiation pressure, because the radial dependence of the radiation forces is fundamentally different. For indirect radiation pressure, expansion causes the radiation force per unit mass to drop faster than R^{-2}, because the flux falls as R^{-2} and the opacity falls as the cloud expands as well. For direct radiation forces, on the other hand, the extremely high opacity of dusty interstellar gas to radiation with the colour temperature of a star ($\kappa \sim 10^3 \, cm^2 \, g^{-1}$) ensures that all photons will be absorbed for any reasonable column of gas. Consequently, the force delivered by the direct radiation field is simply the total momentum flux in the radiation field, which is constant and independent of radius (cf. Thompson et al. 2015). Thus expansion makes gravity stronger compared to the indirect radiation force, but weaker compared to the direct force, and for direct radiation forces expansion is therefore destabilizing rather than stabilizing.

Examining Fig. 2, it is clear that clouds that begin their evolution with surface densities $\Sigma_0 < \Sigma_{0,crit}$ (i.e. with trajectories above the red line in the upper panel and below the red line in the lower panel) will be unbound by direct radiation pressure without ever

being unstable against indirect radiation pressure, while clouds with $\Sigma_0 > \Sigma_{0,crit}$ (with an example shown by the green curve in upper and lower panels of Fig. 2) will either be disrupted by indirect radiation pressure (under our 'type A' assumption) or will be forced to expand by indirect radiation pressure to surface density $\Sigma_{0,crit}$ (under our 'type B' assumption), after which the cloud will continue to form stars at constant surface density until it is disrupted by direct radiation pressure.[13] We show examples of both types of cloud trajectories in Fig. 2.

For type B evolutionary trajectories, where the cloud expands if it becomes unstable to indirect radiation pressure, the final star formation efficiency and surface density are always dictated by the total surface density of the cloud when it encounters the line of direct radiation pressure instability; this is $\Sigma_{tot} = \min(\Sigma_0, \Sigma_{0,crit})$, with the first case corresponding to clouds that begin their evolution at low surface density, $\Sigma_0 < \Sigma_{0,crit}$, and the latter to clouds that begin their lives at high surface density, $\Sigma_0 > \Sigma_{0,crit}$. In either case, we can calculate the final star formation efficiency and stellar surface density analytically, simply by making the substitution $\Sigma_\star = \varepsilon_f \Sigma_{tot}$ in equation (26) and solving. The result is

$$\epsilon_f = \frac{1}{1 + \Sigma_{*,char,dir}/\min\left(\Sigma_0, \Sigma_{0,crit}\right)} \quad (27)$$

$$\Sigma_f = \frac{\min\left(\Sigma_0, \Sigma_{0,crit}\right)}{1 + \Sigma_{*,char,dir}/\min\left(\Sigma_0, \Sigma_{0,crit}\right)}. \quad (28)$$

The maxima of these two functions occurs for $\Sigma_0 \geq \Sigma_{0,crit}$, and for our fiducial parameter choices and solar metallicity, these maxima are $\varepsilon_f \simeq 0.88$ and $\Sigma_f \simeq 1.3 \times 10^5 \, M_\odot \, pc^{-2}$. For type B trajectories, since the surface density of the final stellar state is different to that of the initial gaseous state, it is useful to define an additional measure of efficiency,

$$\epsilon_{f,\Sigma} = \frac{\Sigma_\star}{\Sigma_0} = \frac{\min\left(1, \Sigma_{0,crit}/\Sigma_0\right)}{1 + \Sigma_{*,char,dir}/\min\left(\Sigma_0, \Sigma_{0,crit}\right)}. \quad (29)$$

Intuitively, the difference between ε_f and $\varepsilon_{f,\Sigma}$ is that the former measures the fraction of the initial gas mass transformed into stars, while the latter measures the ratio of the final stellar surface density to the initial gas surface density; thus, the latter quantity accounts for the effects of expansion. The maximum possible value of $\varepsilon_{f,\Sigma}$ is the same as for ε_f.

For type A trajectories, where we assume clouds disrupt instantaneously if they become unstable to direct radiation pressure, the results for ε_f and Σ_f are identical to the type B case for $\Sigma_0 < \Sigma_{0,crit}$, while for $\Sigma_0 > \Sigma_{0,crit}$ the final stellar surface density and star formation efficiency are given by the solution described in Section 2.2.2.

We show the relationship between Σ_0 and Σ_f for both cases in Fig. 3, and we show the corresponding relationship between Σ_0 and ε_f (or $\varepsilon_{f,\Sigma}$) in Fig. 4. In these plots, we use the numerical value for $\Sigma_{0,crit}$ rather than the analytic approximation, although the two differ only very slightly.

---

[13]For a sufficiently large value of f_{trap}/α_{crit}, or a sufficiently high metallicity, it is possible that the tangent point on the indirect radiation pressure curve could move within the zone of instability for direct radiation pressure, in which case clouds undergoing expansion under the effects of indirect radiation pressure would become vulnerable to disruption by direct radiation pressure before reaching a surface density $\Sigma_{0,crit}$. Since this case would require either very large values of f_{trap} or highly supersolar metallicities, it seems unlikely to be relevant in nature, and thus we do not discuss it further.
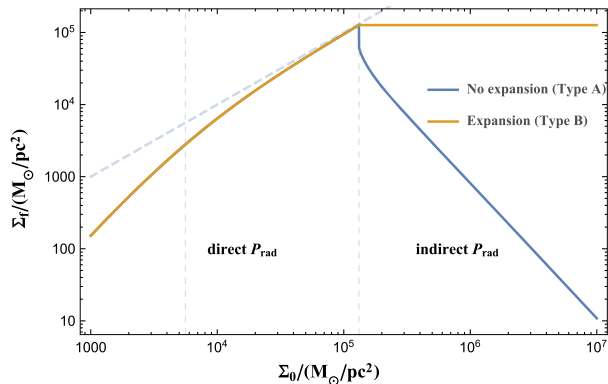
Figure 3. Final stellar surface density Σ_f as a function of initial mass surface density of the star-forming cloud Σ_0 for $\Psi = \Psi_0$. At the low mean surface density end, direct radiation pressure effects (in this case, for fiducial parameters of $\eta = 2/3$ and $f_{trap}/\alpha_{crit} = 1$) limit the final stellar surface density; the left dashed vertical line indicates $\Sigma_{*,char,dir}$ the surface density for which the star formation efficiency permitted by direct radiation pressure is 50 per cent. At the high surface mass density end, indirect radiation pressure effects (in this plot calculated for solar metallicity) constrain the final stellar surface density. The blue curve assumes that the cloud is disrupted when its surface density trajectory intersects the critical curve for indirect radiation pressure (type A trajectory); the yellow curve assumes that the cloud can expand dynamically to maintain marginal stability. The dashed grey curve shows $\Sigma_f = \Sigma_0$. In either case, the model predicts a maximal stellar surface density at $\Sigma_* \sim \Sigma_{0,crit}$, indicated by the right dashed vertical line, though note the expansion case predicts a pile-up at this value whereas the no-expansion case predicts a peak with a downturn on either side of it.
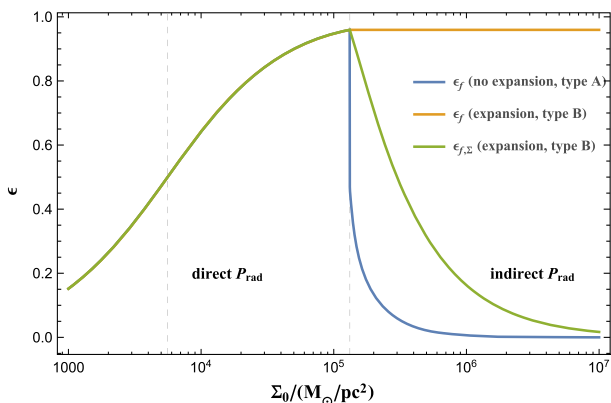

Figure 4. Final star formation efficiency, defined by mass (ε_f) or by surface density ($\varepsilon_{f,\Sigma}$) as indicated in the legend, as a function of initial cloud mass surface density, Σ_0; the curves are calculated using the same parameter values as Fig. 3, and the dashed vertical lines are the same in both cases as well. For the no expansion (type A) case, and for the expansion case with starting surface density $\Sigma_0 < \Sigma_{0,crit}$, both efficiency measures are the same, because the cloud radius does not change during star formation.

3 DISCUSSION

3.1 Limits on surface density: observational comparison

The simple considerations set out above suggest that indirect and direct radiation pressure, acting in concert, should put an upper limit of $\sim 1.3 \times 10^5 \, M_\odot \mathrm{pc}^{-2} \, (Z_\odot/Z) \, (\Psi_0/\Psi)$ for the maximum stellar surface density of star clusters. Interestingly, this finding is broadly

consistent with observations. Indeed, as presaged above, Hopkins et al. (2010) pointed out the apparent existence of an empirical upper bound, at $\Sigma_{max} \sim 10^5 \, M_\odot \, \mathrm{pc}^{-2}$, to the central stellar surface mass density of compact stellar systems. Hopkins et al. (2010) remark that this rough limit holds over a ~ 7 order magnitude range of total mass, a ~ 5 order of magnitude range in physical size, and over ~ 2 orders of magnitude in metallicity. Given this, they tentatively conclude 'that feedback from massive stars likely accounts for the observed Σ_{max}, plausibly because star formation reaches an Eddington-like flux that regulates the growth of these diverse systems'. However, a problem for this explanation – raised by Hopkins et al. (2010) and again recently by Grudić et al. (2018a,b) – is the expectation that Σ_{max} should scale inversely as the metallicity (because of the expectation that the dust-to-gas mass ratio trace metallicity) whereas it did not seem to these authors that there was any such metallicity dependence evident in their data.

Our compilation of the central surface mass density of a number of systems vs metallicity is shown in Fig. 5. The data are still sparsely sampled and subject to selection effects that we have not rigorously characterized. Nevertheless, they do not seem to us to be inconsistent with such a metallicity-dependence for Σ_{max}.

A further point to keep in mind here is that the sloped limit line in Fig. 5 assumes a metallicity independent light to mass ratio $\Psi(Z) \rightarrow \Psi_0$. Where, for instance, the mean IMF to become systematically more 'top heavy' for lower metallicity, this would have the overall effect of attenuating and plausibly even totally cancelling out the metallicity evolution of the critical central surface mass density (cf. recent observations of the 30 Doradus local starburst: Schneider et al. 2018, where the expected ~ 3–4 increase in L/M concomitant with the claimed top-heavy IMF would roughly cancel out the effect of the LMC's $\sim 0.4 \, Z_\odot$). However, we caution the reader that claims for strong metallicity effects on the IMF have frequently been contested or countered with seemingly contradictory examples or analysis (e.g. Bastian, Covey & Meyer 2010; Offner et al. 2014).

Aside from obtaining more data, a fuller empirical analysis of the issue of the putative maximal central surface mass density would have to deal with a number of issues that revolve around questions of systematics connected to the dynamical evolution of stellar systems. One possible confound is that metal-rich GCs tend to have formed nearer the centres of their host galaxies than relatively metal-poor ones, i.e. in a relatively stronger tidal fields. This will render the former more compact at the present time, independent of their initial configuration.

In light of the complexity of applying our model to old stellar systems that may have undergone significant dynamical evolution, the data covering information, embedded superstar clusters in the NGC 253 nuclear starburst obtained by Leroy et al. (2018) provide a particularly interesting test of our model. From ALMA 350 MHz dust continuum observations, these authors find 14 candidate superstar clusters ($M_\star \gtrsim 10^5 \, M_\odot$) within the $\sim 3 \times 10^8 \, M_\odot$ of molecular gas inside NGC 253's nucleus. Each cluster has a large gas fraction and is, consequently, highly extincted behind very high gas and dust columns (yielding optical depths $\tau \sim 5$–10 at 100 μm). Nevertheless, Leroy et al. (2018) find no high-velocity line wings in their data implying that each cluster's gas is gravitationally bound. This finding is broadly consistent with our scenario which suggests that indirect radiation pressure effects in the nascent NGC 253 star clusters, while likely to cause some of the clusters to expand, will not expel the clusters' gas (cf. Fig. 5). Overall, indeed, we would expect a large fraction of each cluster's original gas allocation to be
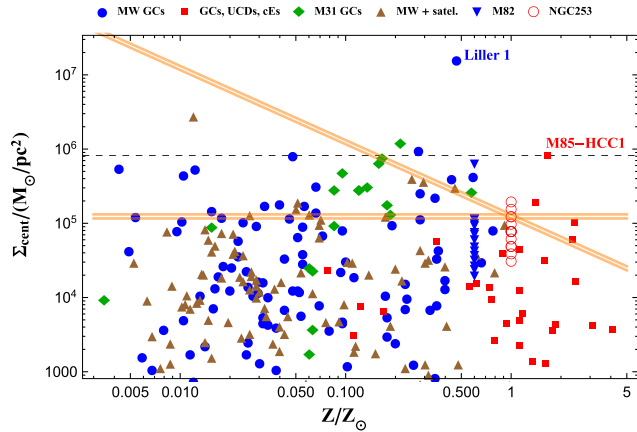
Figure 5. Central surface mass density (measured, inferred, or lower limit as described below) versus metallicity for different compact stellar systems (data truncated below 10^3 M$_\odot$ pc^{-2}). The systems included in the compilation are as follows: *MW GCs:* Milky Way globular clusters ($N = 119$) with central mass surface density from Baumgardt & Hilker (2018) and with metallicities from Harris (1996, 2010); *GCs, UCDs, cEs:* surface mass density within the effective half-light radius for massive globular clusters, ultracompact dwarfs, and compact elliptical galaxies ($N = 29$) from the Archive of Intermediate Mass Stellar Systems with metallicities compiled by Janz et al. (2016); *M31 GCs:* central surface mass densities for globular clusters from M31 ($N = 18$) from the compilation by Barmby et al. (2007); *MW + satel.:* Central surface mass densities for massive clusters from Milky Way and satellites (the Large Magellanic Cloud, Small Magellanic Cloud and the Fornax dwarf spheroidal, $N = 153$) from the compilation by McLaughlin & van der Marel (2005); *M82:* surface density inside half mass radius for superstar clusters from M82 from McCrady & Graham (2007, $N = 15$) adopting gas phase metallicity of 0.6 Z$_\odot$ (Origlia et al. 2004; Nagao et al. 2011); *NGC 253:* total (gas + stars) surface density inside 2D FWHM radius nascent superstar clusters from the central starburst in NGC 253 from Leroy et al. (2018, $N = 14$) adopting gas phase metallicity of 1.0 Z$_\odot$ (Webster & Smith 1983). The sloped orange line is for $\Sigma_{0,\text{crit}}(Z) = \Sigma_{0,\text{crit}}(Z_\odot/Z)$ with $\Psi = \Psi_0$ and a width encompassing the efficient convection and the pure radiative transfer limits (the horizontal orange line is for no metallicity evolution). The dashed horizontal line corresponds (cf. equation 30) roughly to the critical stellar volumetric number density of $n_* \sim 10^6$ pc^{-3} where stellar mergers in cluster cores occur on a timescale less than the main-sequence lifetime of massive stars, allowing the merger formation of giant stars, progenitors of IMBHs (assuming a large fraction of massive stars are in primordial hard binaries; see the text). The two systems that most surpass the expected upper limit are labelled; they are M85-HCC1, a hypercompact star cluster claimed as likely the remnant nucleus of a galaxy recently accreted on to its current host galaxy (Sandoval et al. 2015), and Liller 1, a Galactic globular cluster that is in core collapse (Baumgardt & Hilker 2018).

turned into stars, consistent with the data and analysis presented by Leroy et al. (2018).

3.2 Stellar mergers and IMBHs

A possible consequence of our picture is that clusters formed at higher metallicities (approaching solar) may be prevented by indirect radiation pressure from reaching the volumetric stellar number densities required such that stellar mergers may occur sufficiently rapidly in their cores to form the giant stellar precursors of intermediate-mass black holes (IMBHs). Bonnell & Bate (2005) find that stellar mergers of massive stars can occur on a timescale less than their $\sim 10^6$ yr main-sequence lifetimes – thus allowing for the dynamical formation of giant stars via mergers – for core cluster

densities $n_* \gtrsim 10^6$ pc^{-3} assuming that a large fraction of massive stars are born into hard binary systems. This corresponds to a rough critical surface density

$$\Sigma_{\text{crit,IMBH}} \sim 8 \times 10^5 \, \text{M}_\odot \, \text{pc}^{-2} \left(\frac{M_c}{10^6 \, \text{M}_\odot} \right)^{1/3} \left(\frac{\rho_{\text{crit,IMBH}}}{10^6 \, \text{M}_\odot/\text{pc}^3} \right)^{2/3}. \tag{30}$$

This critical surface density is shown, for the fiducial parameters, as the horizontal dashed line in Fig. 5; compact stellar systems at $Z \gtrsim 0.2 \, Z_\odot$ may have trouble reaching this critical surface density (though it is to be acknowledged that there are a handful of star systems above this rough threshold at $Z \gtrsim 0.2 \, Z_\odot$ in our compilation). This effect is independent of and in addition to stellar mass-loss due to Wolf–Rayet phase winds that also increases as a function of metallicity and may also preclude the formation of IMBHs (Yungelson et al. 2008; Glebbeek et al. 2009).

4 SUMMARY

In this paper, we investigate the combined effects of indirect, dust-reprocessed and direct, stellar radiation pressure on the formation of the densest star clusters. Adopting our calculation from CKTC18 of the largest column of dusty gas for which hydrostatic equilibrium is possible when the column is subject to the opposing forces of indirect radiation pressure and gravity and also drawing results on direct radiation pressure from FKM10, we construct here an evolutionary model for a dense protocluster gas cloud forming stars, and show that clouds with initial surface density $\gtrsim 10^5$ M$_\odot$ pc^{-2} with Milky Way-like dust and dust-to-gas ratios will become super-Eddington with respect to indirect radiation pressure at some point during their star formation process. This effect is unlikely to push gas out of clusters in winds, abruptly cutting-off star formation. Rather, systems with sufficiently high initial surface mass densities probably suffer a rather gentle expansion under indirect radiation pressure effects. Only late in their evolution, once they have typically turned well more than 50 per cent of their original gas allocation into stars, will *direct* radiation pressure effects turn on in such clusters, pushing the remaining gas out of the cluster at greater than the escape speed. This process is complete well before core-collapse supernovae start going off in such clusters.

The combined effect of direct and indirect radiation pressure is to set an upper limit of $\approx 10^5$ ($Z_\odot/Z$) M$_\odot$ pc^{-2} on the surface densities of star clusters, and to produce a star formation efficiency – defined as the ratio of the initial gas surface density to the final stellar surface density – that has a maximum of ≈ 90 per cent for gas clouds with surface densities near this upper limit, and falls off sharply at either lower or higher surface densities. This limit is likely to preclude the formation of IMBHs via stellar collisions in any star cluster with a metallicity above ≈ 20 per cent of solar. The scenario suggested by our model is qualitatively and quantitatively consistent with the empirical determination (Hopkins et al. 2010) that there seems to be an upper limit to the central surface mass density of compact stellar systems at $\sim 10^5$ M$_\odot$ pc^{-2}. We compare our model to an updated compilation of measured stellar surface densities in a wide variety of compact stellar systems, and find that it is qualitatively consistent with the observations, including the possibility that star clusters formed with lower metallicities and thus lower dust content might have systematically higher maximum surface densities. Further tests of this model, and in particular the prediction that the results should depend on metallicity, will require additional measurements of surface densities in low-metallicity systems, preferably

young ones so as to minimize the confounding effects of dynamical evolution.

REFERENCES

Accurso G., 2017, MNRAS, 470, 4750

Andrews B. H., Thompson T. A., 2011, ApJ, 727, 97

Barmby P., McLaughlin D. E., Harris W. E., Harris G. L. H., Forbes D. A., 2007, AJ, 133, 2764

Bastian N., Covey K. R., Meyer M. R., 2010, ARA&A, 48, 339

Baumgardt H., Hilker M., 2018, MNRAS, 478, 1520

Bonnell I. A., Bate M. R., 2005, MNRAS, 362, 915

Chakrabarti S., McKee C. F., 2005, ApJ, 631, 792

Chakrabarti S., McKee C. F., 2008, ApJ, 683, 693

Clarkson W. I., Ghez A. M., Morris M. R., Lu J. R., Stolte A., McCrady N., Do T., Yelda S., 2012, ApJ, 751, 132

Crocker R. M., Krumholz M. R., Thompson T. A., Clutterbuck J., 2018, MNRAS, 478, 81(CKTC18)

Davis S. W., Jiang Y.-F., Stone J. M., Murray N., 2014, ApJ, 796, 107

Fall S. M., Krumholz M. R., Matzner C. D., 2010, ApJ, 710, L142

Glebbeek E., Gaburov E., de Mink S. E., Pols O. R., Portegies Zwart S. F., 2009, A&A, 497, 255

Grudić M. Y., Hopkins P. F., Quataert E., Murray N., 2018a, preprint (arXiv: 1804.04137)

Grudić M. Y., Hopkins P. F., Faucher-Giguère C.-A., Quataert E., Murray N., Kereš D., 2018b, MNRAS, 475, 3511

Harris W. E., 1996, AJ, 112, 1487

Harris W. E., 2010, preprint (arXiv:1012.3224)

Hopkins P. F., Murray N., Quataert E., Thompson T. A., 2010, MNRAS, 401, L19

Janz J. et al., 2016, MNRAS, 456, 617

Kennicutt R. C., Jr, Evans N. J. E., II, 2012, ARA&A, 50, 531

Krumholz M. R., Dekel A., 2010, MNRAS, 406, 112

Krumholz M. R., Matzner C. D., 2009, ApJ, 703, 1352

Krumholz M. R., Thompson T. A., 2012, ApJ, 760, 155

Krumholz M. R., Thompson T. A., 2013, MNRAS, 434, 2329

Lamers H. J. G. L. M., Cassinelli J. P., 1999, in Lamers H. J. G. L. M., Cassinelli J. P., eds, Introduction to Stellar Winds. Cambridge Univ. Press, Cambridge, p. 452

Leroy A. K. et al., 2011, ApJ, 737, 12

Leroy A. K. et al., 2018, preprint (arXiv:1804.02083)

Lopez L. A., Krumholz M. R., Bolatto A. D., Prochaska J. X., Ramirez-Ruiz E., 2011, ApJ, 731, 91

Lopez L. A., Krumholz M. R., Bolatto A. D., Prochaska J. X., Ramirez-Ruiz E., Castro D., 2014, ApJ, 795, 121

McCrady N., Graham J. R., 2007, ApJ, 663, 844

McLaughlin D. E., van der Marel R. P., 2005, ApJS, 161, 304

Massey P., Hunter D. A., 1998, ApJ, 493, 180

Murray N., 2009, ApJ, 691, 946

Murray N., Quataert E., Thompson T. A., 2010, ApJ, 709, 191

Murray N., Ménard B., Thompson T. A., 2011, ApJ, 735, 66

Nagao T., Maiolino R., Marconi A., Matsuhara H., 2011, A&A, 526, A149

Offner S. S. R., Clark P. C., Hennebelle P., Bastian N., Bate M. R., Hopkins P. F., Moraux E., Whitworth A. P., 2014, in Beuther H., Klessen R. S., Dullemond C. P., Henning T., eds, Protostars & Planets VI. Univ. Arizona Press, Tucson, AZ, p. 53

Origlia L., Ranalli P., Comastri A., Maiolino R., 2004, ApJ, 606, 862

Sandoval M. A. et al., 2015, ApJ, 808, L32

Santini P. et al., 2014, A&A, 562, A30

Schneider F. R. N. et al., 2018, Science, 359, 69

Scoville N. Z., Polletta M., Ewald S., Stolovy S. R., Thompson R., Rieke M., 2001, AJ, 122, 3017

Semenov D., Henning T., Helling C., Ilgner M., Sedlmayr E., 2003, A&A, 410, 611

Skinner M. A., Ostriker E. C., 2015, ApJ, 809, 187

Thompson T. A., Krumholz M. R., 2016, MNRAS, 455, 334

Thompson T. A., Quataert E., Murray N., 2005, ApJ, 630, 167

Thompson T. A., Fabian A. C., Quataert E., Murray N., 2015, MNRAS, 449, 147

Tsang B. T.-H., Milosavljević M., 2015, MNRAS, 453, 1108

Tsang B. T.-H., Milosavljević M., 2018, MNRAS, 478, 4142

Webster B. L., Smith M. G., 1983, MNRAS, 204, 743

Wolfire M. G., Cassinelli J. P., 1986, ApJ, 310, 207

Yungelson L. R., van den Heuvel E. P. J., Vink J. S., Portegies Zwart S. F., de Koter A., 2008, A&A, 477, 223

Zhang D., Davis S. W., 2017, ApJ, 839, 54

APPENDIX A: VALIDITY OF THE $\kappa_R \propto T^2$ APPROXIMATION

Our calculation of the critical Eddington ratio $f_{E, crit}$ demarcating stable, sub-Eddington from unstable, super-Eddington behaviour assumes that the temperature $T \lesssim 150$–200 K, so that we can approximate the temperature-dependence of the opacity as $\kappa_R \propto T^2$. Here, we verify that this is in fact the case. In Fig. A1, we plot the reference temperature T_* (equation 6) and the central (i.e. midplane) temperature as calculated in CKTC18 as a function of surface density for marginally stable systems, i.e. for gas clouds with total
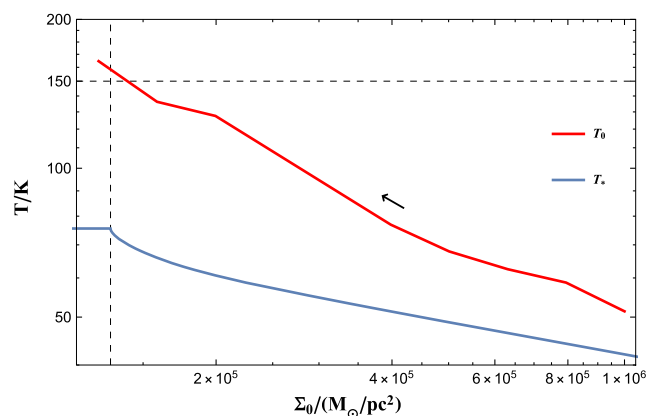

Figure A1. Reference (T_*) and central temperature as a function of total surface density for marginally stable gas clouds. The central temperature is as calculated in CKTC18 for planar geometry. The dashed horizontal line at $T = 150$ K indicates where $\kappa_R(T)$ starts to deviate from a simple $\propto T^2$ behaviour (Semenov et al. 2003). The vertical dashed line indicates $\Sigma_{0, crit}$, the lowest total surface mass density where indirect radiation pressure effects manifest. As indicated by the arrow, systems with $\Sigma_0 > \Sigma_{0, crit}$ evolve from right to left as they process gas into stars while simultaneously expanding (with their core gas heating up). The plot shows that such systems remain in the regime $T < 150$ K over almost the entirety of their evolution.

surface density Σ_0 and gas fraction $f_{\text{gas, crit}} = 1 - \varepsilon_{\text{crit}}(\Sigma_0)$. Note that the $\kappa_R \propto T^2$ behaviour of the opacity breaks down in the temperature range 150–200 K (Semenov et al. 2003), indicated in Fig. A1 by the horizontal dashed line. Systems with $\Sigma_0 > \Sigma_{0,\text{crit}}$ evolve from right to left as they process gas into stars while simultaneously expanding. This plot indicates that, to the extent that it is accurate to treat the geometry in the planar limit, a $\propto T^2$ scaling of $\kappa(T)$ is a very good approximation for most of the evolution of the forming clusters, only (slightly) breaking down as systems approach $\Sigma_{0,\text{crit}}$.

On very small scales around individual stars or stellar systems, of course, the planar approximation must break down, and the radiation temperatures will be higher. However, the scales on which this is the case are *very* small. For example, Wolfire & Cassinelli (1986) show that, even around a 300 M$_\odot$ star with a luminosity of 7×10^6 L$_\odot$, the dust temperature exceeds 200 K only within $\sim 10^3$ au of the source. Even for the very dense star clusters we are considering, this is smaller than the typical separation for such luminous sources. For example, there are ~ 50 early O and WR stars that approach this luminosity in the central ~ 2 pc of R136 (Massey & Hunter 1998), but this still corresponds to a mean interstellar separation $> 10^4$ au. Thus, the forces deposited in the small regions where our approximation $\kappa(T) \propto T^2$ does not apply will not tend to be dynamically dominant, since the forces exerted by different stars will tend to cancel one another.

APPENDIX B: RESULTS FOR CONVECTIVE VERSUS RADIATIVE STABILITY LIMITS

As described in the main text, CKTC18's calculation of the critical surface Eddington ratio $f_{\text{E, crit}}$ at which systems transition from stable and sub-Eddington to unstable and super-Eddington depends weakly on the assumptions one makes about the effectiveness of convective heat transport in fluid where radiation pressure dominates the enthalpy budget, and thus conventional fluid convection
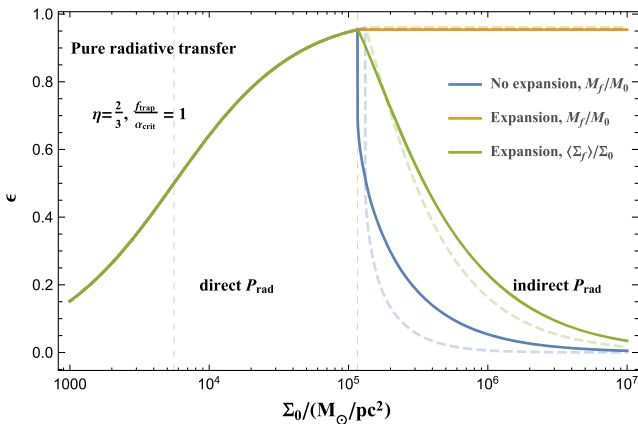

Figure B1. Final star formation efficiency for subregions as a function of initial mass surface density, Σ_0, for the limiting assumptions of efficient versus inefficient convection. This figure is identical to Fig. 4 of the main text, and is calculated identically, except that the solid lines use the stability limit $f_{\text{E, crit}} = f_{\text{E, crit, rt}}$ (inefficient convection) rather than $f_{\text{E,crit}} = f_{\text{E, crit,c}}$ (efficient convection). For comparison, the faint dashed lines show the efficient convection case shown in Fig. 4 of the main text.

is ineffective. All figures shown in the main text, except where noted, are for the 'efficient convection' where one assumes that, despite radiation dominating the enthalpy budget, convection is none the less able to completely flatten the entropy gradient. To justify our assertion that the results would not change qualitatively under the opposite assumption that convection is unable to alter the entropy gradient in this regime, in Fig. B1 we repeat our calculation of the final star formation efficiency using this alternative assumption. In this figure, the solid lines show the case assuming inefficient convection, while the dashed lines show the results assuming efficient convection as in the main text. Clearly, there is little qualitative difference between the results in the two cases.

APPENDIX C: THE EFFECTS OF A CLUMPY GAS DISTRIBUTION

In CKTC18, we did not explicitly consider the effects of gas clumping on the column density, because we could simply envision our calculation as applying locally to every patch of a galactic disc. In spherical geometry, however, the column is necessarily an averaged quantity, and thus we must consider how inhomogeneities in a cloud are likely to affect the gas column density Σ.

Up to the point where the radiation flux becomes large enough to start ejecting gas, variations in Σ will be driven primarily by turbulence. Thus for the purposes of calculating at what point radiation is capable of ejecting mass, the column density distribution that is relevant is the one induced by turbulence, which Thompson & Krumholz (2016) show is well described by a probability distribution function that is approximately lognormal, with a dispersion given by

$$\sigma_{\ln \Sigma}^2 \approx \ln \left(1 + R \mathcal{M}^2 / 4 \right). \tag{C1}$$

Here, $\mathcal{M}$ is the Mach number of the turbulence,

$$R = \frac{1}{2} \left(\frac{3 - \alpha}{2 - \alpha} \right) \left[\frac{1 - \mathcal{M}^{2(2-\alpha)}}{1 - \mathcal{M}^{2(3-\alpha)}} \right], \tag{C2}$$

and $\alpha \approx 2.5$ is the index of the density power spectrum. For such a distribution, the area-weighted median column density is lower than the area-weighted mean by a factor of $\exp\left(-\sigma_{\ln \Sigma}^2 / 2\right)$, while the mass-weighted median is higher by the same factor. For $\mathcal{M} < 100$, this factor is <3.7, i.e. the median column density is within a factor of 4 of the mean column density. Thus, the variations in column density induced by turbulence, as opposed to the variations in volume density, are relatively modest, and comparable to our uncertainties in other quantities (e.g. the dust opacity). Our estimated final column densities should be regarded as uncertain by roughly this factor.

There remains the possibility that these modest variations in column density will have substantially larger effects on the interaction of radiation with the gas, due to preferential escape of photons through low-density regions. However, radiation-hydrodynamic simulations show that this effect is surprisingly small, and does not substantially alter the conditions for gas to be ejected compared to the results of a naive laminar calculation (Davis et al. 2014; Tsang & Milosavljević 2015; Zhang & Davis 2017).

This paper has been typeset from a T$_{\text{E}}$X/L^{A}T$_{\text{E}}$X file prepared by the author.